



# Formation dynamics of SiO<sub>2</sub> nanoparticles produced by laser ablation in ambient gases

R. Koike<sup>1</sup> · R. Suzuki<sup>1</sup> · K. Katayama<sup>1</sup> · M. Higashihata<sup>1</sup> · H. Ikenoue<sup>1,2</sup> · D. Nakamura<sup>1</sup>

Received: 31 May 2022 / Accepted: 4 October 2022 / Published online: 14 October 2022  
© The Author(s), under exclusive licence to Springer-Verlag GmbH, DE part of Springer Nature 2022

## Abstract

Pulsed laser deposition (PLD) is a commonly used technique for fabricating thin films. Additionally, it can produce oxide material nanocrystals and nanoporous films by controlling gas pressure during the deposition. Previously, we fabricated nanoporous films with low dielectric constants by depositing SiO<sub>2</sub> nanoparticles. In such deposition techniques that use laser-generated nanoparticles as raw materials, parameters, such as ambient gas pressure, gas species, and the distance between the target and substrates, have a considerable influence on the size and structure of the nanoparticles. In this study, to clarify the behavior of nanoparticles during pressure-controlled PLD, such as their formation process and spatial distribution, SiO<sub>2</sub> nanoparticles generated by laser ablation are visualized using two-dimensional laser scattering imaging. The spatial distribution of the nanoparticles tends to decrease with increasing ambient gas pressure, and the distribution exhibits various shapes, including spherical and mushroom clouds, depending on the gas species. Nanoparticles generated by laser ablation in the gas phase and collected at different positions from the target surface on a collection substrate placed parallel to the target are observed. Nanoparticles are deposited without aggregation at a collection position below the maximum expansion distance of the laser ablation plasma plume  $l_p$ . In the collected position around and above  $l_p$ , web-like aggregates consisting of nanoparticles with a particle size of a few nanometers are observed. As the pressure increases, the size of the web-like aggregates and number of deposits increase. Information regarding these spatial distributions and deposited aggregates is useful in optimizing conditions, such as ambient gas species, gas pressure, and deposition distance, for nanoporous film fabrication.

**Keywords** Laser ablation · time-resolved imaging · nanoparticles · nanoporous films · pulsed laser deposition

## 1 Introduction

Pulsed laser deposition (PLD) is one of the most promising technologies for the fabrication of various thin films, such as single-wall carbon nanotube composites [1] and superconducting thin films [2, 3]. Laser ablation produces gas-phase particles from a bulk target material; these gas-phase particles are used to fabricate metal nanoparticle [4] and nanoparticle-assisted ZnO nanocrystal [5–7]. Moreover, nanoporous films have reportedly been fabricated using ablation

of SiO<sub>2</sub> crystal substrate targets and deposition of nanoparticles at room-temperature to form low dielectric constant (low-k) insulating films [8]. The SiO<sub>2</sub> nanoporous films have attracted attention in the ultra-large-scale integrated (ULSI) field as insulating films with low dielectric constant owing to their pores and quantum confinement effects. In the ULSI field, low-k materials are required to reduce wiring delays as the device dimensions become smaller. Efforts to lower the dielectric constant include the development of new materials, such as SiOC [9], SiOCH [10], porous films [11], and air gap insertion [12]. Previously, we fabricated nanoporous films via PLD using SiO<sub>2</sub> as a target by controlling the ambient gas pressure, and achieved a relative permittivity of 1.8 [8]. In such deposition techniques that use laser-generated nanoparticles as the raw material, the distance between target substrates and ambient gas pressure are important parameters because they have a significant effect on the particle size and structure of the nanoparticles. Further, clarifying the behavior of nanoparticles, such as their formation

✉ R. Koike  
koike.reiji.383@s.kyushu-u.ac.jp  
D. Nakamura  
dnakamura@ees.kyushu-u.ac.jp

<sup>1</sup> Graduate School of Information Science and Electrical Engineering, Kyushu University, Fukuoka, Japan

<sup>2</sup> Department of Gigaphoton Next GLP, Kyushu University, Fukuoka, Japan

process and spatial distribution, is essential for establishing the fabrication conditions for such aforementioned deposition technology. This study aims to measure the behavior of laser-generated nanoparticles using a two-dimensional (2D) laser imaging technique [13, 14].

## 2 Experimental setup

The setup for the 2D laser image measurements of SiO<sub>2</sub> nanoparticles is shown in Fig. 1 [14]. SiO<sub>2</sub> nanoparticles were produced by laser ablation of a SiO<sub>2</sub> crystal substrate placed in a rotating holder atop a vacuum chamber filled with Ar or O<sub>2</sub> gas. An ArF excimer laser ( $\lambda = 193$  nm, pulse width  $\tau = 15$  ns, COMPex PRO 102F) was used for the laser ablation. The ablation laser beam was shaped into a 5 mm-diameter circle using an aperture; subsequently, it was focused and irradiated onto a SiO<sub>2</sub> crystal target placed in a vacuum chamber using a lens with a focal length of 300 mm. The ablation fluence was 6 J/cm<sup>2</sup> (5.2 mJ on 0.087 mm<sup>2</sup>) and laser irradiation was performed with a single pulse. The pressure of the ambient gas filling the vacuum chamber was adjusted to a range of 400–2700 Pa. The ambient gas was replaced at each irradiation to eliminate the effect of nanoparticles generated by the previous irradiation. Additionally, the in and out gas flow during laser irradiation was eliminated to reduce the influence of convection currents in the chamber on the generated particles. A Nd: YAG laser ( $\lambda = 355$  nm, pulse width  $\tau = 10$  ns, Quanta-ray GCR-200,

Spectra-Physics) was used as a probe laser to obtain Rayleigh scattered light from the nanoparticles produced by the ablation laser. The probe laser beam was shaped into a sheet with a width of approximately 30 mm using a cylindrical lens and was incident horizontally approximately 2 mm above the SiO<sub>2</sub> target surface. The polarization direction of the probe laser beam was horizontal to the observation plane, considering the Rayleigh scattering characteristics. The irradiation fluence was 0.26 J/cm<sup>2</sup> (32 mJ on 12.3 mm<sup>2</sup>), and the laser irradiation was performed with a single pulse. The scattered light from the SiO<sub>2</sub> nanoparticles was measured using an intensified charge-coupled device (ICCD Roper PI-MAX) camera. The ablation laser, probe laser, and ICCD camera were connected to a pulse generator, and the delay time of each device was controlled. By changing the delay time between probe laser and ablation laser, the temporal variation of the spatial distribution of SiO<sub>2</sub> nanoparticles was observed.

The particles generated in the gas phase by laser ablation were collected on a substrate and observed by transmission electron microscopy (TEM). Further, an energy dispersive X-ray spectroscope (EDS) attached to the TEM instrument was used to analyze the elements. In the particle collection experiment, Ar and O<sub>2</sub> gases were used as the ambient gases, and the gas pressure was adjusted to 20 Pa and 400 Pa. The target was ablated 200 times, and the produced particles were deposited on a collection substrate positioned parallel to the target.

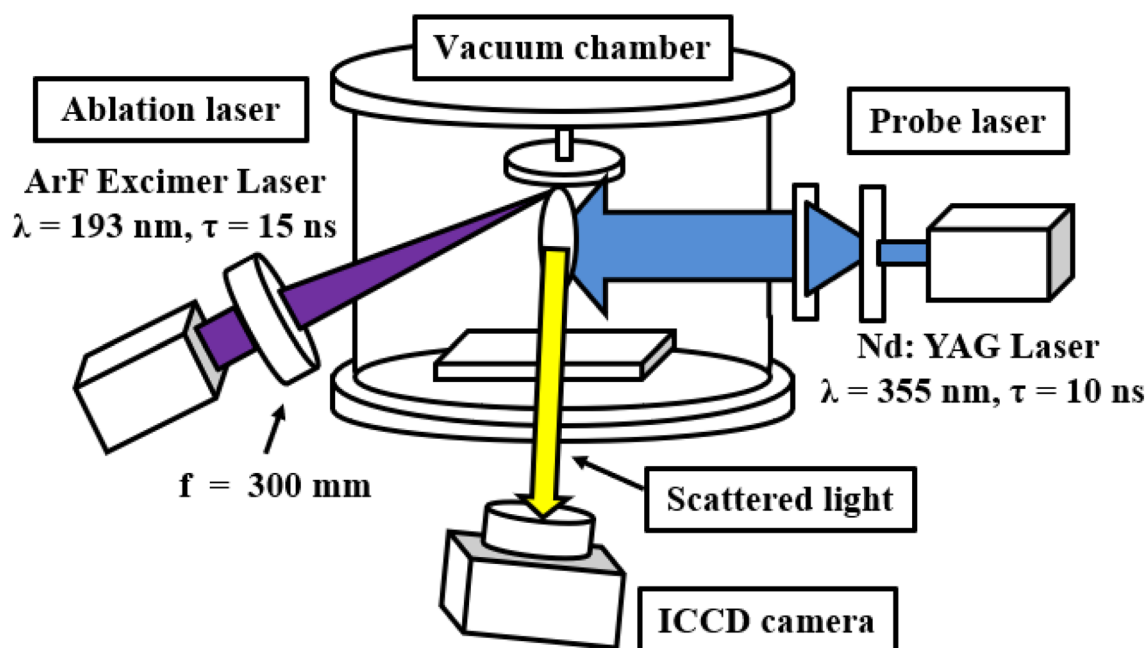


Fig. 1 Experimental setup of the 2D laser imaging system

### 3 Result and discussion

Before measuring the scattered light from the nanoparticles, plasma plume emission produced by laser ablation was observed using the ICCD camera. Plasma plume emission images of O<sub>2</sub> gas at 400 Pa are shown in Fig. 2. The white dotted lines indicate the position of the target surface, and the delay time after the laser irradiation is shown in the lower left corner of each image. The scale bar on the right-hand side of the image indicates the distance from the target surface. Generally, the expansion distance of the plasma plume is represented by the point-blast model [15] described by the following equation.

$$R(t) = \xi(E_0/\rho)^{1/5} t^{2/5} \tag{1}$$

where  $R$ ,  $\xi$ ,  $E_0$ ,  $\rho$ , and  $t$  are the radius of the plasma plume, dimensionless quantity, absorbed energy, ambient gas density, and time after laser irradiation, respectively. Figure 3 shows the time variation of the expansion distance of plasma plume obtained at each gas pressure. The expansion distance

of the plasma plume is defined as the position at which the plasma plume emission intensity is 1/10 of the maximum value at each time. The results obtained in this study are consistent with the theoretical curve of Eq. (1), represented by the solid line. The plasma plume in the O<sub>2</sub> gas at 400 Pa expanded with a gradually decreasing expansion velocity and disappeared after approximately 2  $\mu$ s. Similar plasma images were obtained for Ar and O<sub>2</sub> gases.

After the disappearance of the plasma plume emission, scattered light from the nanoparticles was observed with a delay time of several tens of milliseconds. The spatial distribution images of SiO<sub>2</sub> nanoparticles under different Ar or O<sub>2</sub> gas pressures, namely, 400, 670, 1300, and 2700 Pa were previously observed [16]. Figure 4 shows the scattered light images at a delay time of 800 ms with different pressures of Ar and O<sub>2</sub> gases. In the case of the Ar gas, the spatial distribution of the nanoparticles formed a spherical shape. In contrast, in the case of O<sub>2</sub> gas, the spatial distribution was spherical at 400 Pa, but it changed into a mushroom cloud as the ambient gas pressure increased to 1300 and 2700 Pa. For both gases, the spatial distribution tended to decrease with

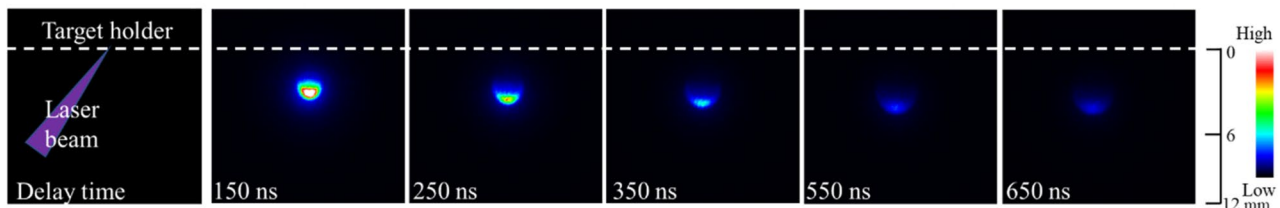
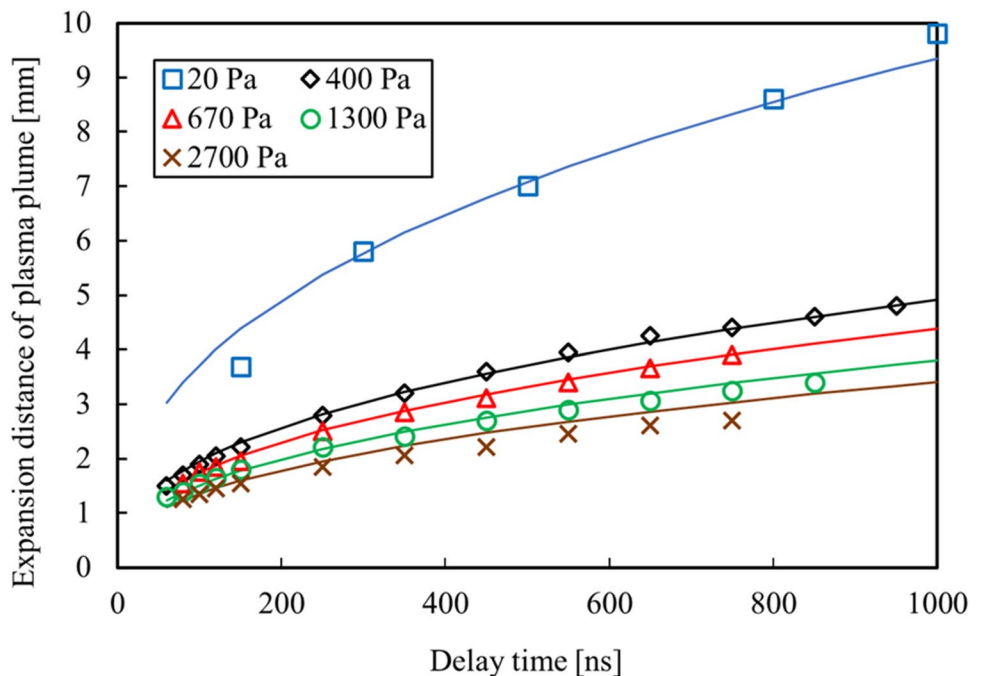
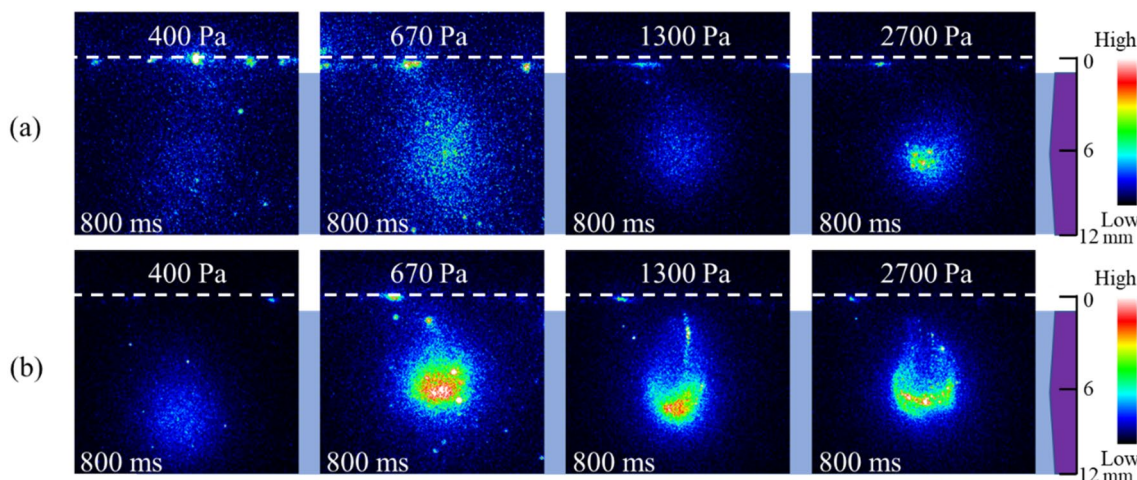


Fig. 2 Laser induced plasma emission images of O<sub>2</sub> gas at 400 Pa

Fig. 3 The expansion distance of the plasma plume in O<sub>2</sub> gas at different pressures





**Fig. 4** Scattered light images from nanoparticles with a delay time of 800 ms at pressures of 400,670,1300, and 2700 Pa of **a** Ar gas and **b** O<sub>2</sub> gas

an increase in ambient gas pressure. These results indicate that the gas species and gas pressure affect the formation and aggregation of the nanoparticles.

Laser-generated nanoparticles are formed by laser-ablated species in the plasma plume owing to the collisions of ambient gas molecules with the species. Therefore, the nanoparticle size and aggregation vary with the distance from the target surface. Herein, we defined the  $D_{TS}$  as the distance from the target surface to particle collection substrate. Representative TEM observations and elemental analysis of Si and O atoms by EDS at  $D_{TS}=4.2$  mm in Ar gas at 400 Pa are shown in Fig. 5. The deposited aggregates consisted of primary particles of approximately 3–5 nm, and the EDS results confirmed that they were composed of Si and O atoms. The TEM images of nanoparticles collected in Ar and O<sub>2</sub> gases at both 20 and 400 Pa are shown in Fig. 6. Evidently, under the same pressure conditions, the structure of the deposited aggregates changed from spherical to web-like as the deposition distance increased. Additionally, web-like

structures were deposited with a smaller  $D_{TS}$  at 400 Pa as compared with 20 Pa. This is believed to be owing to the more active collisions with gas molecules because of the increased gas pressure. As shown in Fig. 7, we defined  $l_p$  as the maximum expansion distance of the plasma plume when the decaying plasma emission can no longer be observed by the ICCD camera. The  $l_p$  was 9.8 mm and 5.7 mm for Ar gas at 20 and 400 Pa, respectively. Whereas it was 10.0 mm and 4.8 mm for the O<sub>2</sub> gas, respectively. Also, we defined the parameter  $L$  as  $L=D_{TS}/l_p$ . The relationship between the deposited aggregates and  $D_{TS}$  can be discussed in three regions shown in Fig. 6:  $L < 1$ ,  $L \sim 1$ , and  $L > 1$ .

The case of the O<sub>2</sub> gas is discussed in this section. For  $L < 1$ , some aggregates consisting of nanoparticles of a few nanometers in diameter were observed; however, the EDS results confirmed the presence of trace amounts of Si and O throughout the observed region. As shown in Fig. 3, the collection substrate was in the region where the plasma plume expanded. In this region, the ablated species were

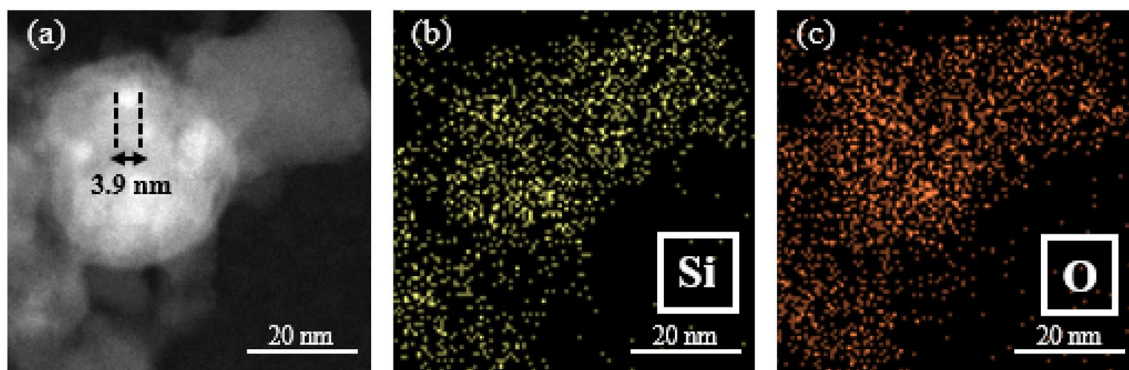


**Fig. 5** **a** Representative TEM image of typical aggregates in Ar gas at 400 Pa. Results of EDS detection of **(b)** Si atoms and **(c)** O atoms

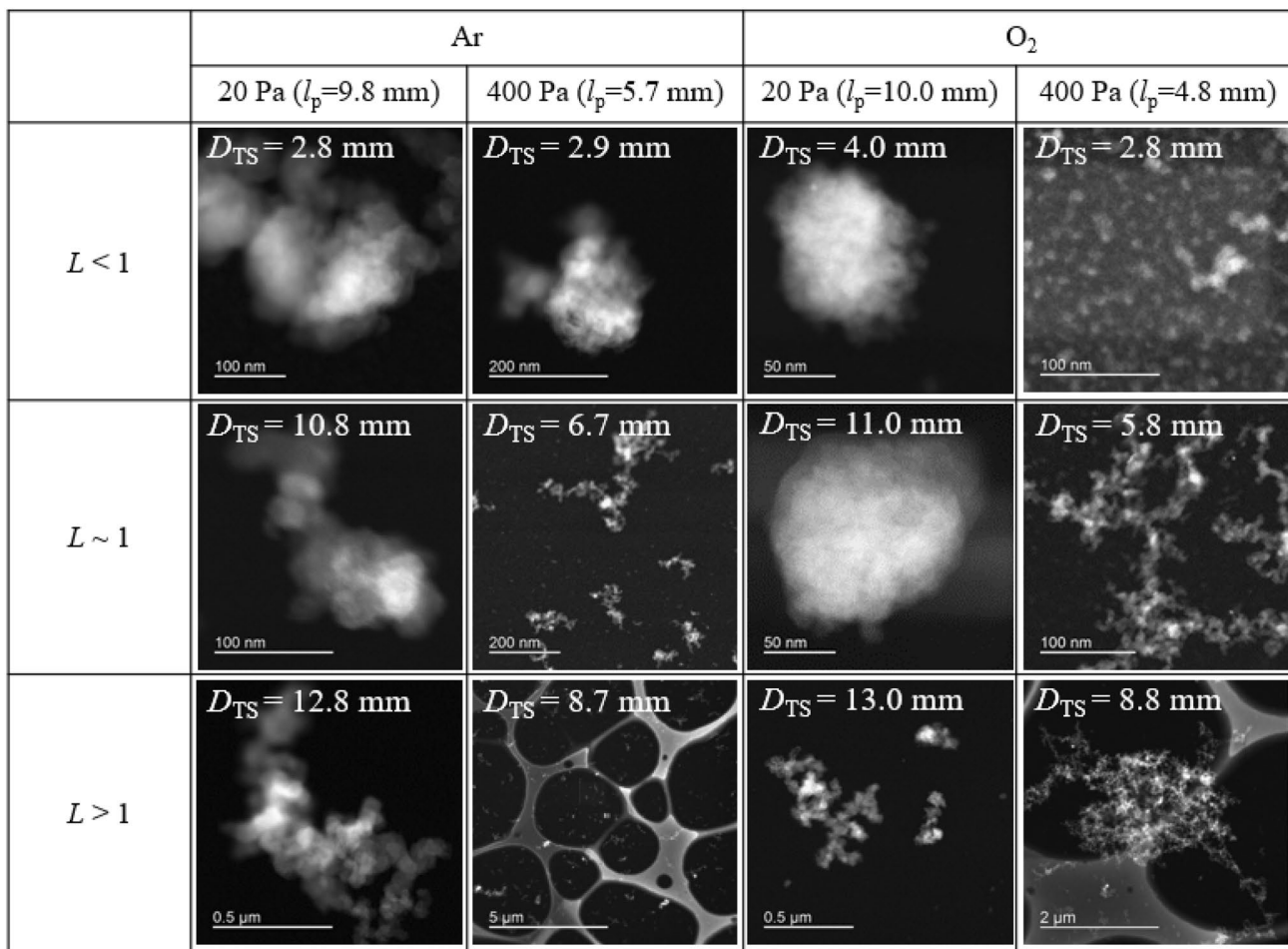


Fig. 6 TEM images of deposited nanoparticles at Ar and O<sub>2</sub> gas pressures of 20 Pa and 400 Pa with different collecting positions *D<sub>TS</sub>*

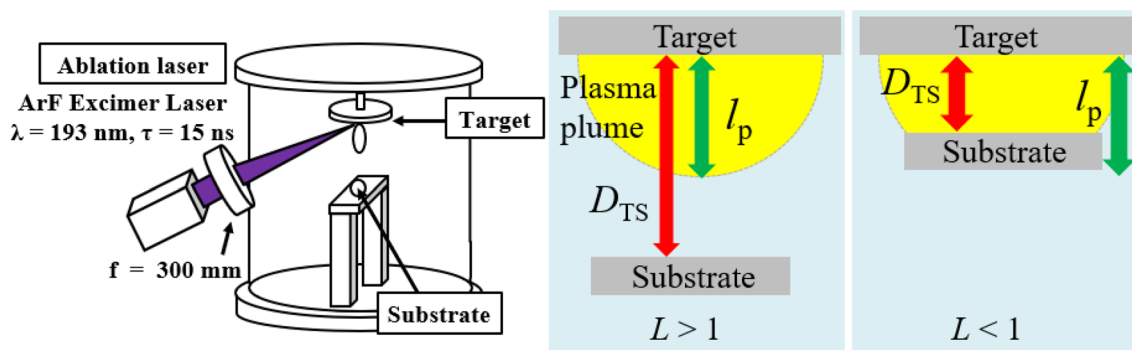
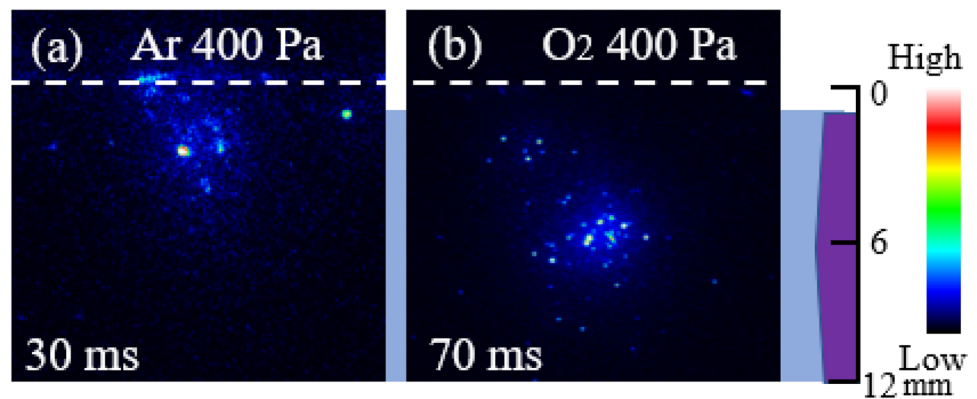


Fig. 7 Setup for particle deposition and definition of *D<sub>TS</sub>*, *l<sub>p</sub>*, *L*

assumed to be deposited on the substrate before aggregation and form thin films. Some of the particles produced by laser ablation were expected to reattach to the target surface and form spherical or web-like aggregates. Because the number of laser irradiations was 200, such aggregates could have

possibly been generated on the target surface during deposition. However, for *L* > 1, a larger number of large web-like aggregates were observed as compared with the other cases. In this region, the plasma plume expanded with the loss of kinetic energy until the internal pressure was equal to

**Fig. 8** Scattered light images of **a** Ar gas and **b** O<sub>2</sub> gas at 400 Pa



the ambient gas pressure. Furthermore, the species in the plasma plume repeatedly collided with ambient gas and formed nanoparticles. The generated nanoparticles moved to the substrate through diffusion in the gas phase. During this process, nanoparticle aggregation occurred in the gas phase and formed web-like aggregates [17, 18]. Web-like aggregates were observed at  $L \sim 1$ . This region is considered an intermediate region between  $L < 1$  and  $L > 1$ .

However, under Ar gas, web-like aggregates were observed, even at  $L < 1$ . In addition, the size and number of aggregates tended to increase as the deposition distance increased, although the number of laser pulse is constant. Therefore, these results indicate that Ar gas may tend to cause aggregation of SiO<sub>2</sub> nanoparticles, or O<sub>2</sub> gas may inhibit aggregation. Further investigations are required to determine whether ambient O<sub>2</sub> gas affects the surface activity of the oxide nanoparticles produced by laser ablation.

Figure 8 shows that scattered light images, which began appearing at 400 Pa of Ar and O<sub>2</sub> gases. As for Ar gas, the scattered light was observed from near the target surface, whereas in the case of O<sub>2</sub> gas, the scattered light was observed at approximately 5 mm above the target surface. These results correspond to the distance at which aggregates were observed by TEM, thereby indicating that the scattered light images represent the spatial distribution of aggregated nanoparticles.

## 4 Conclusion

In this study, the spatial distribution of SiO<sub>2</sub> nanoparticles produced by laser ablation was visualized using 2D laser scattering imaging, and the influence of pressure and gas species on the behavior of the nanoparticles was investigated. Additionally, the shape of the particles as a function of the ambient gas pressure, gas species, and deposition distance was investigated by collecting the particles produced in the gas phase and observing them using TEM. The spatial distribution formed by the nanoparticles tended to decrease

when pressure for both the gases increased. Depending on the gas species, the spatial distribution was spherical or mushroom cloud-like. The shape and aggregation of the deposited particles changed with the ratio  $L$ , which is the distance between the target and substrate to the maximum expansion distance of the plasma plume. As the pressure increased, the size and number of the web-like aggregates tended to increase. A comparison of the TEM observation results with the scattered images revealed that the scattering images captured the spatial distribution of the aggregates of SiO<sub>2</sub> nanoparticles. Information regarding these spatial distributions and deposits is useful in optimizing conditions, such as ambient gas species, gas pressure, and deposition distance, for nanoporous film fabrication.

## References

1. H. Schittenhelm, D.B. Geohegan, G.E. Jellison, A.A. Poretzky, M.J. Lance, P.F. Britt, *Appl. Phys. Lett.* **81**, 2097 (2002)
2. S. Adachi, T. Shimode, M. Miura, N. Chikumoto, A. Takemori, K. Nakao, Y. Oshikubo, K. Tanabe, *Supercond. Sci. Technol.* **25**, 105015 (2012)
3. S.B. Qadri, J.S. Horwitz, D.B. Chrisey, R.C.Y. Auyeung, K.S. Grabowski, *Appl. Phys. Lett.* **66**, 1605 (1995)
4. S.T. Akin, X. Liu, M.A. Duncan, *Chem. Phys. Lett.* **640**, 161 (2015)
5. A.B. Hartanto, X. Ning, Y. Nakata, T. Okada, *Appl. Phys. A* **78**, 299 (2004)
6. K. Okazaki, K. Kubo, T. Shimogaki, D. Nakamura, M. Higashihata, T. Okada, *Adv. Mat. Lett.* **2**, 354 (2011)
7. T. Okada, J. Suehiro, *Appl. Surf. Sci.* **253**, 7840 (2007)
8. R. Miyano, T. Kikuchi, K. Imokawa, D. Nakamura, H. Ikenoue, *Proc. SPIE* **10907**, 109070S (2019)
9. C.C. Chiang, M.C. Chen, L.J. Li, Z.C. Wu, S.M. Jang, M.S. Liang, *J. Electrochem. Soc.* **151**, 612 (2004)
10. K. Maex, M.R. Baklanov, D. Shamiryan, F. Lacopi, S.H. Brongersma, Z.S. Yanovitskaya, *J. Appl. Phys.* **93**, 8793 (2003)
11. S. Iwashita, M. Morita, H. Matsuzaki, K. Koga, M. Shiratani, *Jpn. J. Appl. Phys.* **47**, 6875 (2008)
12. J. Noguchi, T. Oshima, T. Matsumoto, S. Uno, K. Sato, *IEEE Trans. Electron Devices* **56**, 2675 (2009)
13. J. Muramoto, T. Inmaru, Y. Nakata, T. Okada, M. Maeda, *Appl. Phys. A* **69**, 239 (1999)

14. J. Muramoto, Y. Nakata, T. Okada, M. Maeda, *Appl. Surf. Sci.* **127–129**, 373 (1998)
15. N. Arnold, J. Gruber, J. Heitz, *Appl. Phys. A.* **69**, S87 (1999)
16. R. Koike, R. Suzuki, K. Katayama, M. Higashihata, H. Ikenoue, D. Nakamura, *J. Laser Micro. Nanoeng.* **16**, 185 (2021)
17. D. Dellasega, A. Facibeni, F.D. Fonzo, V. Russo, C. Conti, C. Ducati, C.S. Casari, A.L. Bassi, C.E. Bottani, *Appl. Surf. Sci.* **255**, 5248 (2009)
18. A. Maffini, A. Pazzaglia, D. Dellasega, V. Russo, M. Passoni, *Phys. Rev. Mater.* **3**, 083404 (2019)

**Publisher's Note** Springer Nature remains neutral with regard to jurisdictional claims in published maps and institutional affiliations.

Springer Nature or its licensor holds exclusive rights to this article under a publishing agreement with the author(s) or other rightsholder(s); author self-archiving of the accepted manuscript version of this article is solely governed by the terms of such publishing agreement and applicable law.